

Steady-state reaction rate of diffusion-controlled reactions in sheets

Denis S. Grebenkov^{1,*} and Diego Krapf^{2,3,†}

¹*Laboratoire de Physique de la Matière Condensée (UMR 7643),
CNRS – Ecole Polytechnique, University Paris-Saclay, 91128 Palaiseau, France*

²*Electrical and Computer Engineering, Colorado State University, Fort Collins, CO 80523, USA*

³*School of Biomedical Engineering, Colorado State University, Fort Collins, CO 80523, USA*

(Dated: March 17, 2021)

In many biological situations, a species arriving from a remote source diffuses in a domain confined between two parallel surfaces until it finds a binding partner. Since such a geometric shape falls in between two- and three-dimensional settings, the behavior of the macroscopic reaction rate and its dependence on geometric parameters are not yet understood. Modeling the geometric setup by a capped cylinder with a concentric disk-like reactive region on one of the lateral surfaces, we provide an exact semi-analytical solution of the steady-state diffusion equation and compute the diffusive flux onto the reactive region. We explore the dependence of the macroscopic reaction rate on the geometric parameters and derive asymptotic results in several limits. Using the self-consistent approximation, we also obtain a simple fully explicit formula for the reaction rate that exhibits a transition from two-dimensional to three-dimensional behavior as the separation distance between lateral surfaces increases. Biological implications of these results are discussed.

Keywords: Reaction rate; Restricted diffusion; Confinement; Lamina

I. INTRODUCTION

Diffusion is omnipresent in biological systems. In particular, the random motion of ions and molecules in aqueous environments is a critical mechanism responsible for bringing reactants to their reaction centers. Without the effect of actively-driven processes, the concentration C of a species moving with diffusivity D satisfies the diffusion equation

$$\frac{\partial C}{\partial t} = D\Delta C,$$

where $\Delta = \nabla^2$ is the Laplace operator. One should note that the diffusion equation is limited to the case of homogeneous purely viscous liquids and thus it often breaks down in live cells as well as in other complex fluids [1–7], but it is typically an excellent approximation for the motion of small molecules in three dimensions within the range of biologically relevant experimental times [8, 9]. At intermediate time scales, the concentration of most species is often found in steady state and, thus, the diffusion equation simplifies to the Laplace equation

$$\Delta C = 0.$$

In spite of the relative simplicity of this equation, solving it can be non-trivial due to the complex morphology of cellular environments [10–13].

Among the different morphologies that appear within cells, the occurrence of thin interconnected sheets is widespread. For example, two cellular organelles involve the presence of aqueous environments within thin sheets:

mitochondria and the endoplasmic reticulum (ER). On one hand, a mitochondrion contains an outer and an inner membrane that separate this organelle into distinct compartments with different functions, namely an intermembrane space, cristae formed by foldings within the inner membrane and a matrix enclosed by the inner membrane [14]. The intermembrane space is a sheet between the outer and inner membranes of approximately 8 nm in thickness [15, 16]. This compartment has multiple physiological (including its role in oxidative phosphorylation) and pathological functions, and many proteins involved in mitochondrial signaling pathways are specifically targeted to it [17, 18]. On the other hand, the ER is a continuous membrane system with a common enclosed space comprising an intricate three-dimensional network [19–21]. The ER lumen, i.e., its interior, is filled with ions, small molecules, and proteins. In animal cells, the ER is the primary storage site for intracellular Ca^{2+} that can be released as Ca^{2+} signals [22]. Diffusion within the ER lumen is essential for critical cellular processes including protein transport and posttranslational regulation, and quantitative diffusion measurements of Ca^{2+} and proteins therein have been reported [23–25]. The peripheral ER consists of sheets and a network of tubules, where, in mammals, ER sheets are typically in the range of 50 nm in thickness [26].

Besides their occurrence within cell organelles, sheet-shaped structures are common in extracellular spaces where signaling between adjacent cells takes place. These structures are notably prevalent in different brain regions where communication between cells and regulation of extracellular components is of utmost importance for cognitive functions. In particular, the concentrations of K^+ and neurotransmitters such as glutamate are tightly regulated in the extracellular space surrounding neurons. Glutamate, the major excitatory neurotransmitter in the brain of vertebrates, when present in excess

*Electronic address: denis.grebenkov@polytechnique.edu

†Electronic address: diego.krapf@colostate.edu

for extended periods of time, acts as a neurotoxin that triggers cell death. In order to remove excess glutamate, astrocytes take up extracellular glutamate via glutamate transporters so that neurotransmitters are maintained at a low concentration close to resting cells. The best-known region for the action of glutamate transporters in neurotransmitter removal is the synaptic cleft, where astrocytic membranes are observed to wrap the synapse region and express high levels of glutamate transporters [27, 28]. Besides their role in synaptic transmission, astrocytes are also observed to regulate the concentration of neurotransmitters in extrasynaptic and somato-dendritic regions [29, 30]. Furthermore, astrocytic signals are triggered upon binding of glutamate to receptors, which can result in Ca^{2+} signaling and the release of gliotransmitters like glutamate, ATP and D-serine [31]. Most of the processes that regulate glutamate are modulated by glutamate diffusion within extracellular sheets and tunnels. These extracellular spaces are found to have a thickness of the order of 20 nm [32, 33].

In this article, we model how the localization of binding partners alters local concentration within confined sheet-like spaces such as those encountered in the extracellular space or in the peripheral ER. In particular, we investigate the flux associated with the clearing of glutamate from the vicinity of neuronal glutamate receptors. These problems are addressed by solving the three-dimensional reaction-diffusion equations in steady state. The diffusion-limited solution provides an upper bound for the glutamate flux. This is a key aspect in understanding glutamate uptake from the extracellular gap.

The macroscopic reaction rate J of steady-state diffusion-limited reactions has been studied over the last century [34–45]. In the three-dimensional setting, J is often estimated as the Smoluchowski reaction rate on a spherical reactive region of radius ρ ,

$$J_S = 4\pi C_0 D \rho, \quad (1)$$

where C_0 is the concentration of molecules at an (infinitely) distant source [34]. In turn, a steady-state solution in two dimensions is only defined for a source at a finite distance from the reactive region, and the rate J depends on this distance (see below, as well as the related discussion in [39, 40]). Since three-dimensional diffusion between parallel sheets appears to be in between these two conventional cases, the behavior of the reaction rate J is not well understood. The aim of the paper is to determine the dependence of the reaction rate J on the geometric parameters of the problem as such the size of the reactive region, the distance to the source, and the separation between sheets.

The paper is organized as follows. In Sec. II, we present the mathematical model and its solution, and explore the dependence of the reaction rate on the geometric parameters of the problem. In Sec. III, we discuss some limitations of the considered model and the related

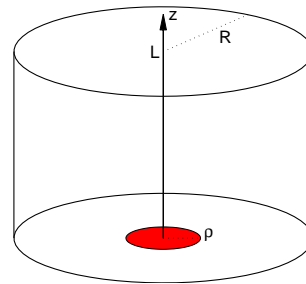


FIG. 1: A disk-like sink of radius ρ (in red) inside the capped cylinder of radius R and of height L . The source of particles is located at the cylindrical surface. In a typical biological setting, one has $R \gg L \gg \rho$ so that the cylinder should be extended in the radial (lateral) direction.

extensions, as well as the biological implications. Technical calculations are reported in Appendices.

II. MATHEMATICAL MODEL AND SOLUTION

We model a thin sheet (e.g., a flat junction between two cells) as a capped cylinder of radius R (the radius of junction) and of height L (the distance between cells), see Fig. 1. In cylindrical coordinates (r, z, φ) , this confining domain is described as

$$\Omega = \{0 < r < R, 0 < z < L, 0 \leq \varphi < 2\pi\}.$$

On one surface (at $z = 0$), there is a target protein that is modeled by a reactive disk Γ of radius ρ . Once a molecule (e.g., glutamate) arrives onto the target protein, it is adsorbed and removed from the domain. We aim at computing the macroscopic reaction rate J , i.e., the steady-state diffusive flux of particles onto the reactive protein coming from outside of the junction. In the steady state, one can assume that multiple sources of particles, distributed in the space outside the junction, maintain the concentration of particles constant at the outer boundary of the junction (i.e., at $r = R$). Fixing the boundary condition at the outer boundary allows one to disentangle the diffusion-reaction problem inside the junction from diffusion in the outer space toward the junction. The latter determines only the constant concentration C_0 at the outer boundary which is just a proportionality factor due to the linear character of the problem. In turn, the solution of the diffusion-reaction problem inside the junction depends on the geometric parameters of the junction: the radius R and the height L of the junction, as well as the radius ρ and the location of the target protein. In this paper, we focus on the role of these geometric factors. We emphasize that this geometric model is different from a model of concentric cylinders with a reactive region on the inner cylinder that was studied in [46, 47] in the context of first passage phenomena. In particular, in our setting, the particles reach the reactive region from above.

In mathematical terms, one needs first to determine the steady-state concentration of particles in the junction, $C(r, z, \varphi)$, by solving the boundary value problem:

$$\Delta C(r, z, \varphi) = 0 \quad \text{in the junction,} \quad (2a)$$

$$C = C_0 \quad \text{on the outer boundary,} \quad (2b)$$

$$C = 0 \quad \text{on reactive region } \Gamma, \quad (2c)$$

$$\partial_n C = 0 \quad \text{on the cell membranes,} \quad (2d)$$

where ∂_n is the normal derivative directed outward the domain. The Dirichlet boundary condition (2c) at the reactive patch expresses a reaction on the target protein upon the first encounter. This perfect reaction can be replaced by a partial reaction modeled by a Robin boundary condition (see Sec. III). Finally, the Neumann boundary condition (2d) ensures that the two lateral surfaces at $z = 0$ and $z = L$, representing the cell membranes, are impenetrable to the particles (except for the reactive region). Once this problem is solved, the diffusive flux onto the reactive region Γ is obtained by integrating the flux density over Γ :

$$J = \int_{\Gamma} ds (-D \partial_n C)|_{\Gamma}. \quad (3)$$

As we are interested in the effect of geometric parameters, it is convenient to compare the flux to the classic Smoluchowski flux J_S from Eq. (1):

$$\Psi = \frac{J}{4\pi C_0 D \rho}. \quad (4)$$

The normalized flux Ψ does not depend on the imposed concentration C_0 . Moreover, there is also no dependence on the diffusion coefficient D for the considered case of perfect steady-state reactions.

When the target protein is located at the center of the surface of one cellular membrane (i.e., it is concentric with the junction, see Fig. 1), the boundary value problem (2) can be solved semi-analytically. In fact, although the solution technique is standard (see Appendix A for details), the resulting expressions for the concentration $C(r, z, \varphi)$ and for the macroscopic reaction rate J are not fully explicit, involving the inversion of an infinite-dimensional matrix. While this step has to be done numerically, the computation is fast and accurate, allowing one to explore the dependence of Ψ on the two geometric ratios L/ρ and R/ρ . Figure 2 shows the normalized flux Ψ as a function of these parameters (note that $R/\rho \geq 1$, whereas L/ρ can range from 0 to ∞). Let us explore the dependence on both geometric parameters.

In the regime $L \ll \rho$, the separation between two lateral boundaries is so short that a particle appearing above the reactive region rapidly reaches this region and reacts. This regime is therefore close to diffusion between two coaxial cylinders of radii R and ρ , for which the concentration profile and the flux are well known:

$$C_{\text{cyl}}(r) = C_0 \frac{\ln(r/\rho)}{\ln(R/\rho)}, \quad J_{\text{cyl}} = \frac{2\pi D L C_0}{\ln(R/\rho)}. \quad (5)$$

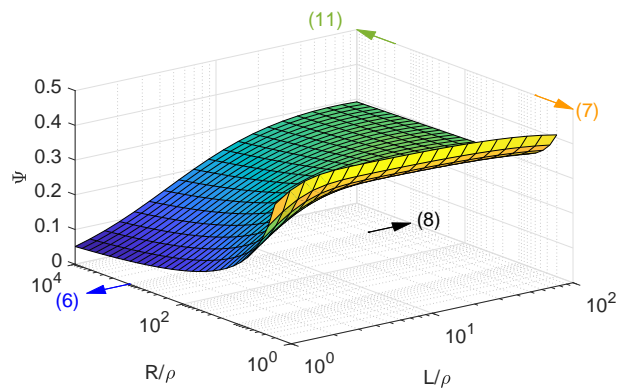


FIG. 2: The normalized flux Ψ as a function of two geometric parameters: L/ρ and R/ρ . For convenience, the practically irrelevant region with $R/\rho \approx 1$ is excluded by setting $R/\rho \geq 2$. The colored arrows indicate the Eq. numbers that show the derived asymptotic relations with their corresponding limits, such as $L/\rho \rightarrow \infty$.

As for the two-dimensional diffusion problem, these solutions vanish logarithmically as $R \rightarrow \infty$. Dividing this flux by J_S , one gets the asymptotic behavior of Ψ as $L \rightarrow 0$:

$$\Psi \simeq \Psi_{\text{cyl}} = \frac{L/\rho}{2 \ln(R/\rho)} \quad (L \ll \rho). \quad (6)$$

In the limit $R \rightarrow \rho$, the concentration $C(r, z, \varphi)$ can be found in a fully explicit form but the diffusive flux diverges logarithmically in this limit (see Appendix A 2 for details):

$$\Psi \rightarrow \frac{1}{\pi} \ln\left(\frac{\rho}{R-\rho}\right) + O(1) \quad (R - \rho \ll \rho). \quad (7)$$

This is a consequence of zero distance between the source (here, the cylinder at $r = \rho$) and the sink (the disk at $z = 0$) that touch each other.

In the limit $L \rightarrow \infty$, the problem is close to that of an absorbing disk in the half-space, for which (see Appendix B):

$$\Psi \simeq \Psi_{\text{disk}} = \frac{1}{\pi} \approx 0.3183 \dots \quad (L \gg R). \quad (8)$$

In this regime, the geometric confinement is irrelevant, and the diffusive flux onto the target protein is close to the Smoluchowski limit. The reduction by the factor π is due to our choice of modeling the target protein by a disk instead of a sphere. To fully illustrate the specific role of the aspect ratio of the reactive region, we compute the normalized flux Ψ for an oblate spheroid, allowing for a continuous variation from a sphere to a disk (see Appendix C).

Unfortunately, the exact semi-analytical solution for $C(r, z, \varphi)$ (Appendix A) is difficult to analyze in the most relevant regime $R \gg L \gg \rho$. Even its numerical computation becomes time consuming because the truncation

size of the infinite-dimensional matrix has to be large. To get a more suitable expression for the flux, we apply the self-consistent approximation (also known as constant-flux approximation) originally devised by Shoup, Lipari and Szabo [48] and then extensively adapted to first-passage time problems [46, 47, 49]. The accuracy of this approximation was investigated in [50]. The approximation consists in replacing the mixed Dirichlet-Neumann conditions (2c, 2d) on the lateral boundary at $z = 0$ by an effective inhomogeneous Neumann condition. The modified boundary value problem is simpler and admits an exact explicit solution (see Appendix D for details). In particular, we derived the following expression for the normalized flux Ψ :

$$\Psi_{\text{sca}} = \frac{\rho}{16R} \left[\sum_{k=0}^{\infty} \frac{J_1^2(\alpha_{0k}\rho/R)}{\alpha_{0k}^3 J_1^2(\alpha_{0k})} \left(1 + \frac{e^{-\alpha_{0k}L/R}}{\sinh(\alpha_{0k}L/R)} \right) \right]^{-1}, \quad (9)$$

where α_{0k} ($k = 0, 1, 2, \dots$) are the positive zeros of the Bessel function $J_0(z)$ of the first kind. The exact solution of the modified problem, Ψ_{sca} , turns out to be a good approximation for the factor Ψ of the original problem, as illustrated by Fig. 3 (compare full and empty symbols). Moreover, this approximation is getting more accurate when ρ is decreased (or R and L are increased), i.e., in the most relevant regime.

Most importantly, the self-consistent approximation provides theoretical insights onto the macroscopic reaction rate. In particular, the monotonous decrease of the function $e^{-z}/\sinh z$ in Eq. (9) implies a monotonous increase of Ψ_{sca} and its approach to a constant as L increases. In other words, a larger separation between lateral boundaries increases the diffusive flux onto the reactive region. Moreover, the two sums in Eq. (9) can be approximately evaluated in the regime $R \gg L \gg \rho$. In fact, the first, slowly converging sum in Eq. (9) can be accurately approximated for $\rho/R \lesssim 0.1$ as

$$\sum_{k=0}^{\infty} \frac{J_1^2(\alpha_{0k}\rho/R)}{\alpha_{0k}^3 J_1^2(\alpha_{0k})} \simeq \frac{2\rho}{3\pi R} + O((\rho/R)^2). \quad (10)$$

In turn, the second sum is exponentially converging so that for small ρ/R , it can be approximated as

$$\frac{\rho^2}{4R^2} \sum_{k=0}^{\infty} \frac{1}{\alpha_{0k} J_1^2(\alpha_{0k})} \frac{e^{-\alpha_{0k}L/R}}{\sinh(\alpha_{0k}L/R)} \approx \frac{\rho^2}{8RL} \ln\left(\frac{R}{2L}\right),$$

where the last approximation is obtained numerically for small L/R . Combining these asymptotic relations, one gets an approximation

$$\Psi_{\text{app}} \simeq \frac{1}{2} \left(\frac{16}{3\pi} + \frac{\rho}{L} \ln\left(\frac{R}{2L}\right) \right)^{-1} \quad (R \gg L \gg \rho). \quad (11)$$

As illustrated in Fig. 3, this approximation is less accurate than Eq. (9) but it is getting more and more accurate as R increases. In contrast to the relation (6)

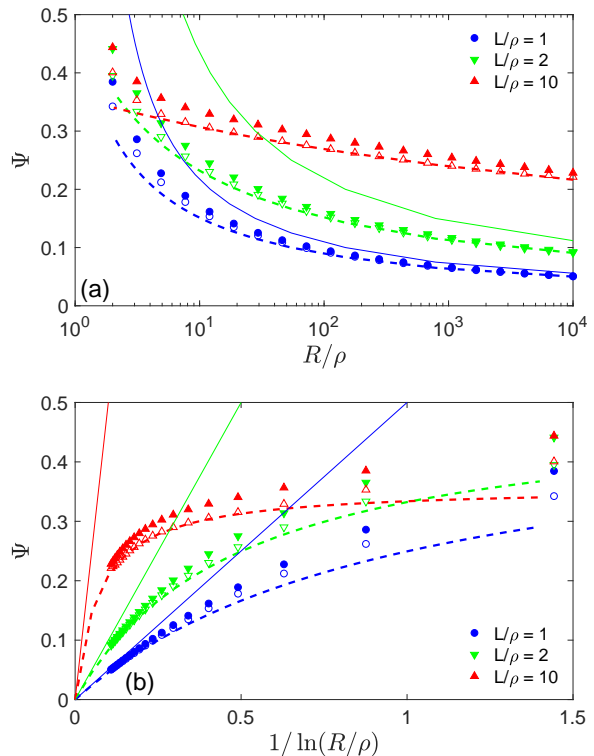


FIG. 3: (a) The normalized flux Ψ as a function of R/ρ , and three values of L/ρ . Full symbols show the exact semi-analytical solution in Eq. (34) obtained by truncating the matrices to the size 500×500 (we also checked that results are very close for truncation to 1000×1000); empty symbols present the self-consistent approximation (9), in which the series is truncated after 10000 terms; thick dashed lines illustrate the explicit approximation (11); thin solid lines indicate Eq. (5) for two co-axial cylinders (note that the red curve corresponding to $L/\rho = 10$ lies above 0.5 and is thus not visible). (b) The same plot shown as a function of $1/\ln(R/\rho)$.

for co-axial cylinders, this explicit approximation captures correctly the dependence of the normalized flux Ψ on both geometric parameters, L/ρ and R/ρ , and can be used to estimate Ψ without resorting to numerical solutions. Note also that the approximation (11) and the expression (6) turn out to be the lower and the upper bounds for the factor Ψ , respectively:

$$\Psi_{\text{app}} \leq \Psi \leq \Psi_{\text{cyl}}. \quad (12)$$

Although we have no rigorous proof for these inequalities, they can be used for a rough estimate of the normalized flux Ψ .

The approximation (11) highlights the main features of the reaction rate J in our geometric setting. In the limit $L \rightarrow \infty$, the factor Ψ_{sca} approaches a constant $3\pi/32 \approx 0.2945$ which is close to the exact value in Eq. (8). In turn, in the limit $R \rightarrow \infty$, the behavior of the factor Ψ_{sca} becomes similar to Eq. (6) for co-axial cylinders, except that the radius ρ of the reactive

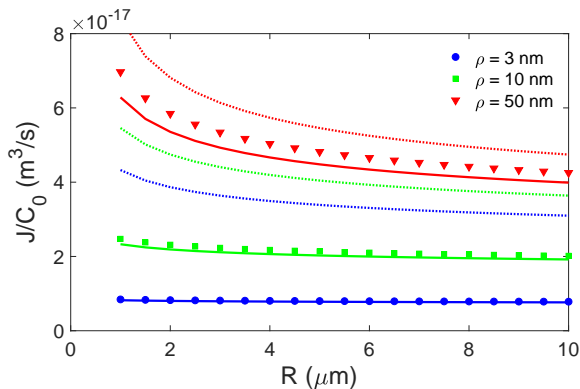


FIG. 4: The diffusive flux J toward the reactive region, normalized by the concentration C_0 at the outer surface, as a function of the outer radius R , with $L = 50$ nm, $D = 800 \mu\text{m}^2/\text{s}$, and three values of ρ : 3 nm (circles), 10 nm (squares), and 50 nm (triangles). Solid lines show our approximation (11), whereas dotted lines indicate Eq. (5) for two co-axial cylinders.

region is replaced by $2L$ under the logarithm. Most importantly, the approach to the latter limit is extremely slow: the constant $A = 16/(3\pi) \approx 1.7$ can be neglected when $R/L \gg 2 \exp(A^{L/\rho})$. For instance, if $L/\rho = 5$, R/L needs to be much larger than 10^6 . In other words, whenever $L/\rho \gtrsim 5$, the co-axial approximation is not applicable, whereas the approximation (11) yields rather accurate results. We emphasize that the limits $L \rightarrow \infty$ and $R \rightarrow \infty$ cannot be interchanged, their order is important.

For illustrative purposes, we compute the diffusive flux J for a realistic set of the model parameters: $D = 800 \mu\text{m}^2/\text{s}$, $L = 50$ nm, $\rho = 3\text{--}50$ nm, and $R = 1\text{--}10 \mu\text{m}$. Figure 4 shows the diffusive flux as a function of the outer radius R for three values of the radius ρ : 3 nm (a single receptor), 10 nm (a small group of receptors), and 50 nm (a large cluster of receptors). In the former case, the flux does not almost depend on the outer radius, as expected for the regime $R \gg L \gg \rho$. In turn, when the inner radius ρ becomes comparable to the inter-cell distance L , a weak dependence on R emerges. One can see that our approximation (11) accurately captures this behavior. For comparison, we also plot the flux from Eq. (5) for two co-axial cylinders. Although this formula reproduces qualitatively the behavior of the flux for ρ comparable to L , it strongly over-estimates the flux for small ρ .

III. DISCUSSION

For a particular geometric shape of a junction (Fig. 1), we obtained the exact semi-analytical solution for the steady-state concentration of particles, diffusing from the outer boundary of the junction to a reactive region on the surface. We focused on the macroscopic reaction rate J

and studied its dependence on three geometric parameters: the radius ρ of the reactive region, and the radius R and height L of the junction. This geometric shape falls in between two commonly studied limits: unrestricted diffusion in three-dimensional space ($L, R \rightarrow \infty$) and two-dimensional diffusion ($L \rightarrow 0$). We showed that none of the conventional expressions for the reaction rate is applicable in the intermediate regime $R \gg L \gg \rho$, which is the most relevant for many biological applications. Using the self-consistent approximation, we managed to derive an explicit simple approximation for the reaction rate J . For a fixed $L \gg \rho$, this approximation highlights the extremely slow decay of the reaction rate with the junction radius R . On one hand, the very weak dependence on R suggests that this parameter is irrelevant. On the other hand, one cannot fully get rid of this parameter by setting $R \rightarrow \infty$ (as in the conventional three-dimensional case) because the reaction rate would vanish.

The derivation of both semi-analytical solution and self-consistent approximation relied on modeling the target protein by a reactive disk located at the center of the lateral surface. While this assumption may look oversimplistic, one can argue that the shape and location of the reactive region are not relevant in the regime $R \gg L \gg \rho$. For instance, the normalized flux Ψ changes from $1/\pi \approx 0.32$ for a disk to 0.5 for a half-sphere in the half-space ($L, R \rightarrow \infty$). Even if L is not infinitely large, the dependence on the shape is expected to be weak. Similarly, the displacement of the reactive region from the center of the lateral surface would change the distance $R - \rho$ from the source to this region. If this distance is still much larger than L and ρ , the reaction rate should not be much affected (see the related discussion in Ref. [51] for planar diffusion, for which an explicit solution can be obtained by a conformal mapping even for a non-concentric reactive region; see also [52] and references therein for other diffusion-reaction applications of conformal mapping).

Another simplification consisted in considering perfect reactions occurring immediately upon the first encounter with the reactive region. In practice, a particle arriving onto the reactive region has to overcome an energetic barrier to form a complex, and may fail to react and thus resume its diffusive motion. This mechanism of imperfect reactions can be accounted for via a finite reactivity κ in the Robin boundary condition on the reactive region [35, 38, 53–57]. For instance, the Smoluchowski reaction rate J_S is reduced by the factor $1 + D/(\kappa\rho)$ for imperfect reactions [35]. Both the semi-analytical solution and self-consistent approximation can be easily adapted to this problem (see Appendices A and D for details). In particular, applying the same analysis to the self-consistent approximation (76), one can extend the approximation (11) to imperfect reactions

$$\Psi_{\text{app}} \simeq \frac{1}{2} \left[\frac{2D}{\kappa\rho} + \frac{16}{3\pi} + \frac{\rho}{L} \ln\left(\frac{R}{2L}\right) \right]^{-1} \quad (R \gg L \gg \rho). \quad (13)$$

As for a small sphere in \mathbb{R}^3 , the binding process with the disk-like reactive region becomes reaction-limited as $\rho \rightarrow 0$ or $\kappa \rightarrow 0$, with the dominant term $2D/(\kappa\rho)$, independently of other geometric parameters. Even if the reaction mechanism is relatively fast so that the term $2D/(\kappa\rho)$ is of order 1, its presence can significantly affect the reaction rate. This highlights the importance of accounting for imperfect reaction mechanisms and potential pitfalls of considering reactions as perfect. Note that we have put forward perfect reactions for clarity of presentation, bearing in mind the provided extensions for the imperfect case.

Finally, we focused on a single reactive site located on the lateral surface. In biological applications, there are typically many reactive sites distributed over the surface. Even if these sites are well separated from each other, the total diffusive flux is not equal to the flux to a single site multiplied by the number of sites. In fact, reactive sites compete for capturing the diffusing particles that yields long-range diffusive interactions between reactive sites [58–60]. Moreover, the reactive region located closer to the outer source can (partly) screen the reactive sites in the central region [51, 53, 61]. As a consequence, the analysis of the steady-state diffusion equation with multiple reactive regions is much more involved and often relies on numerical solutions. Since this problem is beyond the scope of the paper, we only mention that a region of the lateral surface covered by uniformly distributed reactive sites can be modeled as a large partially reaction region. In this homogenized problem, the partial reactivity κ accounts for eventual reflections of diffusing particles on passive regions of the lateral surface.

We have solved explicitly the diffusion to capture problem within a sheet. This problem is particularly relevant to the diffusion of signaling molecules within organelles and to that of glutamate and other neurotransmitters in the brain extracellular spaces. The problem is solved semi-analytical as a function of reactive region size, sheet thickness, and radial distance to the source. Besides the exact solutions, simple expressions for the thin- and thick-sheet asymptotics as well as the large radial distance-to-source are provided. Some biologically-relevant conclusions are obtained. In particular, even though the flux is monotonically decreasing with the radial distance-to-source, the flux decay is very slow, making the reaction rate practically insensitive to this distance. Thus, it is possible for a cell system to dramatically reduce the area devoid of reactive sites without a substantial effect on the adsorption flux. Another important result is shown for the effect of the sheet thickness. For very thin sheets, when the thickness is smaller than the radius of the reactive region, the flux is proportional to the sheet thickness and practically insensitive to that radius. Thus in this system, the flux to capture to a single protein is in essence the same as that of capture to a cluster of molecules and, as a consequence, the cell would not gain anything by increasing the number of target proteins within a single site. On the other hand, for large

sheet thicknesses, the flux is proportional to the radius of the reactive region. Finally, the solution to the case where both the diffusion and adsorption rate play roles, i.e., for the imperfect reaction is also provided. This case is particularly relevant for glutamate transporters that are known to be limited by the velocity of glutamate transport across the astrocytic membrane.

Acknowledgments

DG acknowledges the support under Grant No. ANR-13-JSV5-0006-01 of the French National Research Agency.

APPENDICES

A. SEMI-ANALYTICAL SOLUTION

In this Appendix, we provide the mathematical derivation of the macroscopic reaction rate on the target protein (the reactive region Γ), which is located at the center of the surface, i.e., it is concentric with the junction domain Ω : $\Gamma = \{0 < r < \rho, z = 0\}$. As a consequence, one can drop the dependence on the angular coordinate φ , and the boundary value problem (2) becomes

$$\left(\partial_r^2 + \frac{1}{r}\partial_r + \partial_z^2\right)u(r, z) = 0, \quad (14a)$$

$$u|_{r=R} = 1, \quad (14b)$$

$$u|_{z=0} = 0 \quad (0 < r < \rho), \quad (14c)$$

$$(\partial_z u)|_{z=0} = 0 \quad (\rho < r < R), \quad (14d)$$

$$(\partial_z u)|_{z=L} = 0, \quad (14e)$$

from which $C(r, z, \varphi) = C_0 u(r, z)$. While the problem is classic, the mixed Dirichlet-Neumann boundary conditions (14c, 14d) present the major technical difficulty.

To overcome this difficulty, it is convenient to split the domain Ω into two parts: $\Omega_1 = \{0 < r < \rho, 0 < z < L\}$ and $\Omega_2 = \{\rho < r < R, 0 < z < L\}$. In the inner part Ω_1 , we search a solution in the form satisfying Eqs. (14a, 14c, 14e):

$$u_1(r, z) = \sum_{n=1}^{\infty} c_n^{(1)} v_n^{(1)}(r) \sin(\alpha_n^{(1)} z/L), \quad (15)$$

with $\alpha_n^{(1)} = \pi(n - 1/2)$,

$$v_n^{(1)}(r) = \frac{I_0(\alpha_n^{(1)} r/L)}{I_0(\alpha_n^{(1)} \rho/L)}, \quad (16)$$

$c_n^{(1)}$ are unknown coefficients, and $I_\nu(z)$ are the modified Bessel functions of the first kind. In the outer part Ω_2 , we search a solution in the form satisfying Eqs. (14a,

14b, 14d, 14e):

$$u_2(r, z) = 1 + c_0^{(2)} \ln(r/R) + \sum_{n=1}^{\infty} c_n^{(2)} v_n^{(2)}(r) \cos(\alpha_n^{(2)} z/L), \quad (17)$$

where $\alpha_n^{(2)} = \pi n$,

$$v_n^{(2)}(r) = K_0(\alpha_n r/L) - I_0(\alpha_n r/L) \frac{K_0(\alpha_n R/L)}{I_0(\alpha_n R/L)}, \quad (18)$$

$c_n^{(2)}$ are unknown coefficients, and $K_\nu(z)$ are the modified Bessel functions of the second kind.

The unknown coefficients can be determined by matching two solutions at $r = \rho$:

$$u_1(\rho, z) = u_2(\rho, z), \quad (19a)$$

$$(\partial_r u_1(r, z))|_{r=\rho} = (\partial_r u_2(r, z))|_{r=\rho}. \quad (19b)$$

Substituting u_1 and u_2 into the first relation, multiplying by $\sin(\alpha_m^{(1)} z/L)$ and integrating over z from 0 to L , one gets an infinite system of linear equations,

$$\frac{2}{\alpha_m^{(1)}} (1 + c_0^{(2)} \ln(\rho/R)) + \sum_{n=1}^{\infty} c_n^{(2)} v_n^{(2)}(\rho) B_{nm} = c_m^{(1)} \quad (20)$$

for each $m = 1, 2, \dots$, where we used that $v_m^{(1)}(\rho) = 1$, and B is the infinite-dimensional matrix with elements

$$\begin{aligned} B_{nm} &= \frac{2}{L} \int_0^L dz \sin(\alpha_m^{(1)} z/L) \cos(\alpha_n^{(2)} z/L) \\ &= \frac{2\alpha_m^{(1)}}{[\alpha_m^{(1)}]^2 - [\alpha_n^{(2)}]^2}, \end{aligned} \quad (21)$$

because $\cos \alpha_n^{(1)} = \sin \alpha_n^{(2)} = 0$. Note that

$$BB^\dagger = I, \quad B^\dagger B = I + C, \quad (22)$$

where I is the identity matrix, \dagger denotes the matrix transposition, and

$$C_{mn} = -\frac{2}{\alpha_m^{(1)} \alpha_n^{(1)}}. \quad (23)$$

Next, substituting u_1 and u_2 into Eq. (19b), multiplying by $\cos(\alpha_m^{(2)} z/L)$ and integrating over z from 0 to L , one gets another infinite system of linear equations,

$$c_m^{(2)} (\partial_r v_m^{(2)}(r))|_{r=\rho} = \sum_{n=1}^{\infty} c_n^{(1)} (\partial_r v_n^{(1)}(r))|_{r=\rho} B_{mn} \quad (24)$$

with $m = 1, 2, \dots$. Finally, the integral of Eq. (19b) over z from 0 to L yields

$$c_0^{(2)} = \rho \sum_{n=1}^{\infty} \frac{c_n^{(1)} (\partial_r v_n^{(1)}(r))|_{r=\rho}}{\alpha_n^{(1)}}. \quad (25)$$

Combining these equations, one gets a closed infinite system of linear equations for unknowns $c_n^{(1)}$:

$$\begin{aligned} c_m^{(1)} &= \frac{2}{\alpha_m^{(1)}} + \frac{2\rho \ln(\rho/R)}{\alpha_m^{(1)}} \sum_{n=1}^{\infty} c_n^{(1)} \frac{(\partial_r v_n^{(1)}(r))|_{r=\rho}}{\alpha_n^{(1)}} \\ &+ \sum_{n=1}^{\infty} c_n^{(1)} (\partial_r v_n^{(1)}(r))|_{r=\rho} \sum_{n'=1}^{\infty} B_{n'n} \frac{v_{n'}^{(2)}(\rho)}{(\partial_r v_{n'}^{(2)}(r))|_{r=\rho}} B_{n'm}. \end{aligned}$$

Introducing diagonal matrices

$$V_{mn}^{(1)} = \delta_{mn} \frac{1}{L (\partial_r v_n^{(1)}(r))|_{r=\rho}}, \quad (26)$$

$$V_{mn}^{(2)} = \delta_{mn} \frac{v_n^{(2)}(\rho)}{L (\partial_r v_n^{(2)}(r))|_{r=\rho}}, \quad (27)$$

one can rewrite the above equations in a matrix form as

$$\mathbf{c}^{(1)} = 2\mathbf{b} + (\eta C + B^\dagger V^{(2)} B) (V^{(1)})^{-1} \mathbf{c}^{(1)}, \quad (28)$$

where

$$\mathbf{b}_n = \frac{1}{\alpha_n^{(1)}}, \quad \eta = (\rho/L) \ln(R/\rho), \quad (29)$$

and the matrix C is defined by Eq. (23). One gets thus

$$c_m^{(1)} = 2[V^{(1)} X \mathbf{b}]_m, \quad (30)$$

where

$$X = (V^{(1)} - (\eta C + B^\dagger V^{(2)} B))^{-1}. \quad (31)$$

From Eq. (24), one also gets

$$c_m^{(2)} = \frac{2}{L (\partial_r v_m^{(2)}(r))|_{r=\rho}} [B X \mathbf{b}]_m, \quad (32)$$

while $c_0^{(2)}$ is given according to Eq. (25) as

$$c_0^{(2)} = \frac{2\rho}{L} (\mathbf{b} \cdot X \mathbf{b}). \quad (33)$$

The found coefficients $c_n^{(1)}$ and $c_n^{(2)}$ fully determine the solution $u(r, z)$ of the boundary value problem (14). Figure 5 shows the concentration profile $u(r, z)$ for a reactive disk of radius $\rho = 1$. One can see how the concentration drops from 1 at the outer cylinder (at $r = R = 10$) to 0 at the reactive region.

The diffusive flux onto the reactive region reads

$$\begin{aligned} J &= 2\pi C_0 D \int_0^\rho dr r (\partial_z u_1(r, z))_{z=0} \\ &= 2\pi C_0 D \rho \sum_{n=1}^{\infty} c_n^{(1)} \frac{I_1(\alpha_n^{(1)} \rho/L)}{I_0(\alpha_n^{(1)} \rho/L)} \\ &= 2\pi C_0 D \rho \sum_{n=1}^{\infty} c_n^{(1)} \frac{L (\partial_r v_n^{(1)}(r))|_{r=\rho}}{\alpha_n^{(1)}} \\ &= 4\pi C_0 D \rho (\mathbf{b} \cdot X \mathbf{b}). \end{aligned}$$

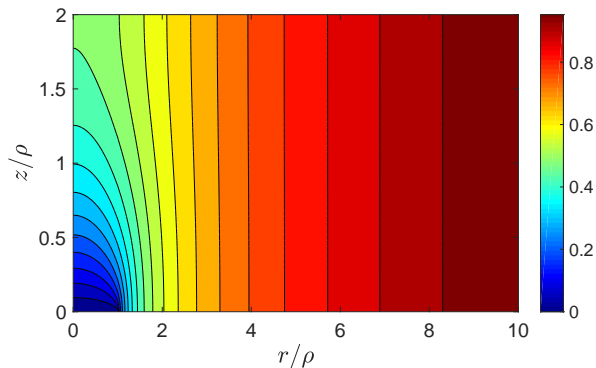


FIG. 5: Concentration $u(r, z)$ for $\rho = 1$, $R = 10$, and $L = 2$.

Dividing this expression by the Smoluchowski flux in Eq. (1), one finds the normalized flux Ψ accounting for the shape of the domain:

$$\Psi = (\mathbf{b} \cdot X \mathbf{b}). \quad (34)$$

By construction, Ψ is equal to 1 for a reactive sphere of radius ρ in the three-dimensional space. In our setting, the normalized flux is a function of two geometric parameters, R/ρ and L/ρ .

While the above solution of the boundary value problem (14) and the consequent expression (34) for the normalized flux Ψ are exact, they involve the inversion of an infinite-dimensional matrix in Eq. (31) that requires numerics. For this reason, the presented solution is called semi-analytical. In practice, one needs to truncate infinite-dimensional matrices and vectors and then to compute numerically the normalized flux Ψ and thus the flux J . The accuracy of this computation is controlled by the truncation size and can be easily verified. Although the dependence on the geometric parameters R/ρ and L/ρ is “hidden” by the matrix inversion, this semi-analytical solution is easily computable and thus allows one to explore the shape dependence.

1. Limit $R \rightarrow \infty$

In the limit $R \rightarrow \infty$, one has

$$v_n^{(2)}(r) = K_0(\alpha_n^{(2)} r/L), \quad (35)$$

so that

$$V_{mn}^{(1)} = \delta_{mn} \frac{I_0(\alpha_n^{(1)} \rho/L)}{\alpha_n^{(1)} I_1(\alpha_n^{(1)} \rho/L)}, \quad (36)$$

$$V_{mn}^{(2)} = -\delta_{mn} \frac{K_0(\alpha_n^{(2)} \rho/L)}{\alpha_n^{(2)} K_1(\alpha_n^{(2)} \rho/L)}. \quad (37)$$

While all the matrices remain well defined in this limit, the factor η in the matrix X in Eq. (31) diverges logarithmically. Qualitatively, one can thus expect that the matrix X vanishes logarithmically as well.

To clarify this point, we consider the regime $L \ll \rho$, for which

$$\begin{aligned} V_{mn}^{(1)} &\longrightarrow (V_0^{(1)})_{mn} = \frac{\delta_{mn}}{\alpha_n^{(1)}}, \\ V_{mn}^{(2)} &\longrightarrow (V_0^{(2)})_{mn} = -\frac{\delta_{mn}}{\alpha_n^{(2)}} \end{aligned}$$

(this is also true in the limit $n \rightarrow \infty$).

In a first attempt, one can try to neglect all matrices in the expression (31) for X , except for the dominant term $-\eta C$. However, such an approximation is useless as the matrix C is not invertible. For this reason, we neglect only the matrix $\mathcal{B}^\dagger V^{(2)} B$. In fact, one can show that this matrix is asymptotically comparable to the matrix C and thus can be neglected as compared to C due to the large factor η in front of C . The remaining matrix $V^{(1)} - \eta C$, truncated to the size $N \times N$, can be inverted explicitly, i.e.,

$$\tilde{X}_{mn}^{(N)} = \left[(V^{(1)} - \eta C)^{-1} \right]_{mn} = \delta_{mn} \alpha_n^{(1)} - \frac{2\eta}{1 - 2\eta A_N}, \quad (38)$$

where $A_N = 1/\alpha_1^{(1)} + \dots + 1/\alpha_N^{(1)}$ (the sign tilde highlights that this is an approximation, in which the matrix $\mathcal{B}^\dagger V^{(2)} B$ was neglected). As a consequence, the normalized flux Ψ becomes

$$\Psi_N = \frac{A_N}{1 + 2\eta A_N}. \quad (39)$$

In the limit $N \rightarrow \infty$, the series of $1/\alpha_k^{(1)}$ diverges logarithmically, i.e., $A_N \rightarrow \infty$, from which we retrieve the normalized flux Ψ for two co-axial cylinders:

$$\Psi_N \rightarrow \Psi_{\text{cyl}} = \frac{1}{2\eta} = \frac{L/\rho}{2 \ln(R/\rho)}. \quad (40)$$

This is expected because the geometric setting $R \gg \rho \gg L$ resembles to two-dimensional diffusion. However, getting corrections to this limit due to the matrix $\mathcal{B}^\dagger V^{(2)} B$ is a difficult, technically involved problem which is beyond the scope of the paper.

2. Limit $R \rightarrow \rho$

When $R \rightarrow \rho$, the outer subdomain Ω_2 shrinks. Setting $R = \rho(1 + \varepsilon)$, the first-order expansions in powers of ε are

$$\eta \simeq \rho\varepsilon/L, \quad V_{mn}^{(2)} = -\delta_{mn} \rho\varepsilon/L, \quad (41)$$

so that

$$X = (V^{(1)} + (\rho\varepsilon/L)I)^{-1}. \quad (42)$$

As a consequence, Eq. (30) implies that $c_n^{(1)} \rightarrow 2/\alpha_n^{(1)}$ as $\varepsilon \rightarrow 0$ and thus

$$u(r, z) = u_1(r, z) = 2 \sum_{n=1}^{\infty} \frac{v_n^{(1)}(r)}{\alpha_n^{(1)}} \sin(\alpha_n^{(1)} z/L). \quad (43)$$

Moreover, Eq. (34) yields the diffusive flux and the factor Ψ :

$$\Psi = \sum_n \frac{1}{(\alpha_n^{(1)})^2} \left(\frac{\rho \varepsilon}{L} + \frac{I_0(\alpha_n^{(1)} \rho/L)}{\alpha_n^{(1)} I_1(\alpha_n^{(1)} \rho/L)} \right)^{-1}. \quad (44)$$

This relation shows that the diffusive flux diverges logarithmically with ε . We checked numerically that

$$\Psi \simeq -\frac{1}{\pi} \ln \varepsilon + O(1) \quad (\varepsilon \rightarrow 0), \quad (45)$$

with $\varepsilon = (R - \rho)/\rho$, and the constant term depending on ρ/L . The divergence of the flux also follows from a direct computation of J from the exact solution in Eq. (43). In mathematical terms, the divergence is related to the fact that at the circle $\{r = \rho, z = 0\}$, the boundary conditions $C = C_0$ at $r = \rho$ and $C = 0$ at $z = 0$ contradict to each other.

3. Extension to partial reactivity

When the target protein is partially reactive (i.e., when the reaction does not occur immediately upon the arrival onto the reactive region), the Dirichlet boundary condition (14c) should be replaced by a more general Robin boundary condition

$$[D(\partial_z u) - \kappa u]_{|z=0} = 0 \quad (0 < r < \rho), \quad (46)$$

where κ is the reactivity [35, 38, 53–57], which can vary from 0 (no reaction) to infinity (perfect reaction, as considered in the main text). This extension affects only the solution (15) in the inner subdomain, in which $\sin(\alpha_n^{(1)} z/L)$ is replaced by $\cos(\alpha_n^{(1)} (L - z)/L)$, where $\alpha_n^{(1)}$ are now obtained as solutions of the trigonometric equation:

$$\frac{D}{\kappa L} \alpha_n^{(1)} \sin \alpha_n^{(1)} = \cos \alpha_n^{(1)}. \quad (47)$$

This change also affects the computation of the matrix B for which Eq. (21) is replaced by

$$B_{nm} = \frac{2\alpha_m^{(1)} \sin \alpha_m^{(1)}}{[\alpha_m^{(1)}]^2 - [\alpha_n^{(2)}]^2}. \quad (48)$$

B. DISK IN THE HALF-SPACE

In the double limit $L \rightarrow \infty$ and $R \rightarrow \infty$, the problem is reduced to the classic problem of electrified disk in the (half)-space, for which the solution was found by Weber (see [62], p. 64). In our notations, the solution in the upper half-space reads

$$u(r, z) = 1 - \frac{2}{\pi} \int_0^\infty \frac{d\mu}{\mu} \sin(\mu\rho) e^{-\mu z} J_0(\mu r). \quad (49)$$

This function satisfies the Laplace equation with the mixed boundary conditions on the plane $z = 0$:

$$\begin{aligned} u(r, z)|_{z=0} &= 0 \quad (0 \leq r < \rho), \\ (\partial_z u(r, z))|_{z=0} &= 0 \quad (r > \rho), \end{aligned} \quad (50)$$

and $u(r, z) \rightarrow 1$ as $r \rightarrow \infty$ or $z \rightarrow \infty$. The flux density is then

$$\begin{aligned} j(r) &= DC_0 \frac{2}{\pi} \int_0^\infty d\mu \sin(\mu\rho) J_0(\mu r) \\ &= \frac{2DC_0}{\pi \sqrt{\rho^2 - r^2}} \quad (0 \leq r < \rho), \end{aligned} \quad (51)$$

whereas the diffusive flux is obtained by integration over the disk:

$$J_{\text{disk}} = 4DC_0\rho. \quad (52)$$

We retrieved thus the particular case of the Hill formula [63]. The flat shape of the disk reduces the factor Ψ from 1/2 for a half-sphere to $\Psi_{\text{disk}} = 1/\pi \approx 0.3183$.

C. SOLUTION FOR AN OBLATE SPHEROID

As we mentioned in Appendix B, the particular choice of the reactive region as a disk reduces the factor Ψ . In order to illustrate the dependence on the shape of the reactive region, we recall the solution of the steady-state diffusion equation for an oblate spheroid in \mathbb{R}^3 (see Fig. 6). It is natural to use the oblate spheroidal coordinates (μ, θ, φ) which are related to the Cartesian coordinates via

$$\begin{aligned} x &= a \cosh \mu \cos \theta \cos \varphi, \\ y &= a \cosh \mu \cos \theta \sin \varphi, \\ z &= a \sinh \mu \sin \theta, \end{aligned} \quad (53)$$

whereas

$$\begin{aligned} \cosh \mu &= \frac{d_+ + d_-}{2a}, \\ \cos \theta &= \frac{d_+ - d_-}{2a}, \\ \tan \varphi &= y/x, \end{aligned} \quad (54)$$

with $d_\pm = \sqrt{(\rho \pm a)^2 + z^2}$, $\rho = \sqrt{x^2 + y^2}$. Here μ varies from 0 to infinity, θ from $-\pi/2$ to $\pi/2$, and φ from 0 to 2π . Note that the oblate spheroid at a constant μ_0 is obtained by rotating ellipses about the z -axis. An ellipse in the $x - z$ plane has a major semiaxis of length $a \cosh \mu_0$ along the x -axis, whereas its minor semiaxis has length $a \sinh \mu_0$ along the z -axis. The foci of all the ellipses in the $x - z$ plane are located on the x -axis at $\pm a$. In other words, if the major and minor semiaxes are denoted as a_\pm , one has $a = \sqrt{a_+^2 - a_-^2}$ and $\mu_0 = \tanh^{-1}(a_-/a_+)$.

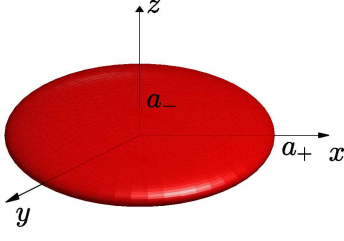


FIG. 6: Oblate spheroid with major and minor semiaxes a_+ and a_- .

Harmonic functions can be decomposed onto the following regular and singular functions

$$\begin{cases} P_n^m(i \sinh \mu) P_n^m(\sin \theta) e^{im\phi} & (\text{regular}), \\ Q_n^m(i \sinh \mu) P_n^m(\sin \theta) e^{im\phi} & (\text{singular}), \end{cases}$$

where P_n^m and Q_n^m are the Legendre functions of the first and second kind, respectively. Since we are interested in a solution outside the oblate spheroid, we use only singular functions. Due to the symmetry of the boundary conditions, there is only the contribution from $m = n = 0$, i.e.,

$$u = 1 - \frac{Q_0(i \sinh \mu)}{Q_0(i \sinh \mu_0)}, \quad (55)$$

where μ_0 determines the boundary $\partial\Omega$ of the oblate spheroid, and $Q_0(z) = \frac{1}{2} \ln\left(\frac{z+1}{z-1}\right)$. This function solves the following problem

$$\begin{aligned} \Delta u &= 0 & (\mu > \mu_0), \\ u|_{\partial\Omega} &= 0 & (\mu = \mu_0), \\ u|_{\|x\| \rightarrow \infty} &\rightarrow 1. \end{aligned} \quad (56)$$

Note that

$$Q_0(iz) = -\frac{i}{2} \cos^{-1}\left(\frac{z^2 - 1}{z^2 + 1}\right), \quad (57)$$

so that

$$\begin{aligned} Q_0(i \sinh \mu) &= -\frac{i}{2} \cos^{-1}\left(1 - \frac{2}{\cosh^2 \mu}\right) \\ &= -\frac{i}{2} \cos^{-1}\left(\frac{(d_+ + d_-)^2 - 8a^2}{(d_+ + d_-)^2}\right). \end{aligned} \quad (58)$$

The flux density onto the oblate spheroid is then

$$\begin{aligned} j &= -C_0 D (\partial_n u)|_{\partial\Omega} = \left(\frac{C_0 D}{h_\mu} \partial_\mu u\right)|_{\mu=\mu_0} \\ &= -\frac{C_0 D i}{h_{\mu_0} \cosh \mu_0 Q_0(i \sinh \mu_0)}, \end{aligned} \quad (59)$$

where $h_\mu = a \sqrt{\sinh^2 \mu + \sin^2 \theta}$. The diffusive flux is then

$$J = \int_{\Gamma} d\theta d\phi h_\theta h_\phi j \quad (60)$$

$$= 2\pi C_0 D a \int_{-\pi/2}^{\pi/2} d\nu \frac{i \cos \theta}{Q_0(i \sinh \mu_0)} = \frac{4\pi C_0 D a i}{Q_0(i \sinh \mu_0)},$$

where $h_\theta = a \sqrt{\sinh^2 \mu + \sin^2 \theta}$ and $h_\phi = a \cosh \mu$. Using the relation $\mu_0 = \tanh^{-1}(a_-/a_+)$ and Eq. (58), one gets

$$Q_0(i \sinh \mu_0) = -\frac{i}{2} \cos^{-1}\left(\frac{2a_-^2}{a_+^2} - 1\right) = -i \cos^{-1}(a_-/a_+). \quad (61)$$

One retrieves thus the explicit form of the diffusive flux discussed in [64]

$$J = 4\pi C_0 D \frac{\sqrt{a_+^2 - a_-^2}}{\cos^{-1}(a_-/a_+)}. \quad (62)$$

In particular, one gets $J = 8C_0 D a_+$ in the limit $a_- \rightarrow 0$, as expected for the disk of radius a_+ . In the limit $a_- \rightarrow a_+$, one can write $a_- = a_+(1 - \varepsilon)$ and then $\cos^{-1}(1 - \varepsilon) \simeq 2\sqrt{\varepsilon}$, so that the Smoluchowski rate is retrieved. Dividing the flux by the Smoluchowski rate for a sphere of radius a_+ , one gets

$$\Psi_{\text{oblate}} = \frac{\sqrt{1 - (a_-/a_+)^2}}{\cos^{-1}(a_-/a_+)}, \quad (63)$$

which varies from $2/\pi$ at $a_-/a_+ = 0$ (the disk) to 1 at $a_-/a_+ = 1$ (the sphere). This factor should be halved if one considers a half of an oblate spheroid in the half-space.

D. SELF-CONSISTENT APPROXIMATION

We also provide an approximate but explicit solution to the problem based on the self-consistent approximation originally developed by Shoup, Lipari and Szabo [48] and then extensively adapted to first-passage time problems [46, 47, 49]. Within the self-consistent approximation, the Dirichlet boundary condition at the target protein is replaced by an approximate Neumann condition with an unknown constant flux density \hat{j} . In other words, the mixed Dirichlet-Neumann boundary conditions (14c, 14d) are replaced by inhomogeneous Neumann condition

$$D(\partial_z \hat{u})|_{z=0} = \hat{j} \Theta(\rho - r), \quad (64)$$

where Θ is the Heaviside step function. The solution of the modified boundary value problem (14a, 14b, 14e, 64), denoted as \hat{u} , can be expressed through the Green function $G(\mathbf{x}, \mathbf{x}')$ in the capped cylinder:

$$\hat{u}(\mathbf{x}) = 1 - \frac{\hat{j}}{D} \int_{\Gamma} d\mathbf{x}' G(\mathbf{x}, \mathbf{x}'), \quad (65)$$

where Γ is the reactive region, and $\mathbf{x} = (r, z, \varphi)$ in cylindrical coordinates. The Green function satisfies

$$-\Delta_{\mathbf{x}}G(\mathbf{x}, \mathbf{x}') = \delta(\mathbf{x} - \mathbf{x}'), \quad (66)$$

subject to the Dirichlet boundary condition $G(\mathbf{x}, \mathbf{x}') = 0$ at $r = R$, and Neumann boundary conditions $\partial_z G(\mathbf{x}, \mathbf{x}') = 0$ at $z = 0$ and $z = L$. The latter can be expressed via the corresponding Laplacian eigenfunctions

$$G(\mathbf{x}, \mathbf{x}') = \sum_{m,n,k} \lambda_{mnk}^{-1} u_{mnk}(\mathbf{x}) u_{mnk}^*(\mathbf{x}'), \quad (67)$$

where

$$\begin{aligned} u_{mnk}(r, z, \varphi) &= c_{mnk} J_n(\alpha_{nk} r/R) \cos(\pi m z/L) e^{in\varphi}, \\ \lambda_{mnk} &= \alpha_{nk}^2/R^2 + \pi^2 m^2/L^2, \end{aligned}$$

with $m = 0, 1, \dots$, $n = 0, 1, \dots$, $k = 0, 1, \dots$, and c_{mnk} are the normalization constants,

$$c_{mnk} = \frac{\epsilon_m}{\sqrt{\pi L R^2} J_{n+1}(\alpha_{nk})} \quad (68)$$

(with $\epsilon_m = \sqrt{2}$ for $m > 0$, and $\epsilon_0 = 1$), and α_{nk} are the positive zeros of the Bessel function $J_n(z)$. We get thus

$$\begin{aligned} \hat{u}(r, z) &= 1 - \frac{\hat{j}}{D} \sum_{m,n,k} \lambda_{mnk}^{-1} u_{mnk}(r, z, \varphi) \int_0^\rho dr' r' \int_0^{2\pi} d\varphi' u_{mnk}^*(r', 0, \varphi') \\ &= 1 - \frac{2\pi\hat{j}}{D} \sum_{m,k} \frac{c_{m0k}^2}{\lambda_{m0k}} J_0(\alpha_{0k} r/R) \cos(\pi m z/L) \int_0^\rho dr' r' J_0(\alpha_{0k} r'/R) \\ &= 1 - \frac{2\pi\hat{j}}{D} \sum_{m,k} \frac{c_{m0k}^2}{\lambda_{m0k}} J_0(\alpha_{0k} r/R) \cos(\pi m z/L) \frac{\rho J_1(\alpha_{0k} \rho/R)}{\alpha_{0k}/R} \\ &= 1 - \frac{2\hat{j}\rho}{DLR} \sum_{m,k} \frac{\epsilon_m^2}{\lambda_{m0k}} \frac{J_0(\alpha_{0k} r/R) J_1(\alpha_{0k} \rho/R)}{\alpha_{0k} J_1^2(\alpha_{0k})} \cos(\pi m z/L). \end{aligned}$$

Using the identity for $0 \leq x \leq 1$,

$$\sum_{m=1}^{\infty} \frac{\cos(\pi m x)}{(\pi m)^2 + z^2} = \frac{\cosh z(1-x)}{2z \sinh z} - \frac{1}{2z^2}, \quad (69)$$

one can evaluate the sum over m that yields

$$\begin{aligned} \hat{u}(r, z) &= 1 - \frac{2\hat{j}\rho}{D} \sum_k \frac{J_0(\alpha_{0k} r/R) J_1(\alpha_{0k} \rho/R)}{\alpha_{0k}^2 J_1^2(\alpha_{0k})} \\ &\quad \times \frac{\cosh \alpha_{0k}(L-z)/R}{\sinh \alpha_{0k} L/R}. \end{aligned} \quad (70)$$

The yet unknown flux density \hat{j} is determined by imposing that the solution \hat{u} satisfies the Dirichlet boundary condition *on average*, i.e.,

$$0 = \int_{\Gamma} d\mathbf{x} \hat{u}|_{z=0}, \quad (71)$$

from which

$$\frac{\hat{j}}{D} = \frac{1}{4R} \left(\sum_k \frac{J_1^2(\alpha_{0k} \rho/R)}{\alpha_{0k}^3 J_1^2(\alpha_{0k})} \operatorname{ctanh}(\alpha_{0k} L/R) \right)^{-1}. \quad (72)$$

Multiplying this flux density by the area of the reactive region, one determines the diffusive flux of particles in the modified problem:

$$\hat{J} = C_0 \pi \rho^2 \hat{j}. \quad (73)$$

From this flux, one gets Eq. (9) for the normalized flux Ψ .

In the case of imperfect reactions, one uses the same inhomogeneous Neumann condition (64) to substitute the mixed Robin-Neumann boundary conditions (14d, 46). As a consequence, the solution (70) of the modified problem remains the same, whereas the average Dirichlet condition (71) determining the effective flux density \hat{j} is replaced by

$$0 = \int_{\Gamma} d\mathbf{x} \left(\hat{u} - \frac{D}{\kappa} \partial_z \hat{u} \right) |_{z=0}, \quad (74)$$

from which

$$\frac{\hat{j}}{D} = \frac{1}{4R} \left(\frac{D}{4\kappa R} + \sum_k \frac{J_1^2(\alpha_{0k}\rho/R)}{\alpha_{0k}^3 J_1^2(\alpha_{0k})} \operatorname{ctanh}(\alpha_{0k}L/R) \right)^{-1} \quad (75)$$

and thus

$$\Psi_{\text{sca}} = \frac{1}{2} \left(\frac{2D}{\kappa\rho} + \frac{8R}{\rho} \sum_k \frac{J_1^2(\alpha_{0k}\rho/R)}{\alpha_{0k}^3 J_1^2(\alpha_{0k})} \operatorname{ctanh}(\alpha_{0k}L/R) \right)^{-1}. \quad (76)$$

-
- [1] J.-P. Bouchaud and A. Georges, Anomalous diffusion in disordered media: statistical mechanisms, models and physical applications, *Phys. Rep.* **195**, 127-293 (1990).
- [2] J. Klafter and I. M. Sokolov, Anomalous diffusion spreads its wings, *Physics world*, **18**, 29 (2005).
- [3] J.-H. Jeon, V. Tejedor, S. Burov, E. Barkai, C. Selhuber-Unkel, K. Berg-Sørensen, L. Oddershede, and R. Metzler, In vivo anomalous diffusion and weak ergodicity breaking of lipid granules, *Phys. Rev. Lett.* **106**, 048103 (2011).
- [4] R. Metzler, J.-H. Jeon, A. G. Cherstvy, and E. Barkai, Anomalous diffusion models and their properties: non-stationarity, non-ergodicity, and ageing at the centenary of single particle tracking, *Phys. Chem. Chem. Phys.* **16**, 24128-24164 (2014).
- [5] I. M. Sokolov, Models of anomalous diffusion in crowded environments, *Soft Matter* **8**, 9043-9052 (2012).
- [6] G. Guigas and M. Weiss, Sampling the cell with anomalous diffusion: the discovery of slowness, *Biophys. J.* **94**, 90-94 (2008).
- [7] D. Krapf, Mechanisms underlying anomalous diffusion in the plasma membrane, *Curr. Topics Membr.* **75**, 167-207 (2015).
- [8] M. B. Elowitz, M. G. Surette, P. E. Wolf, J. B. Stock, and S. Leibler, Protein Mobility in the Cytoplasm of *Escherichia coli*, *J. Bacteriology* **181**, 197-203 (1999).
- [9] A. S. Verkman, Solute and macromolecule diffusion in cellular aqueous compartments. *Trends Biochem. Sci.* **27**, 27-33 (2002).
- [10] H. S. Carslaw and J. C. Jaeger, *Conduction of Heat in Solids*, 2nd Ed. (Oxford University Press, 1959).
- [11] S. Redner, *A Guide to First Passage Processes* (Cambridge: Cambridge University press, 2001).
- [12] O. Bénichou, C. Chevalier, J. Klafter, B. Meyer, and R. Voituriez, Geometry-controlled kinetics. *Nature Chem.* **2**, 472-477 (2010).
- [13] O. Bénichou and R. Voituriez, From first-passage times of random walks in confinement to geometry-controlled kinetics, *Phys. Rep.* **539**, 225-284 (2014).
- [14] T. G. Frey and C. A. Mannella, The internal structure of mitochondria, *Trends Biochem. Sci.* **25**, 319-324 (2000).
- [15] L. F. van Driel, J. A. Valentijn, K. M. Valentijn, R. I. Koning, and A. J. Koster, Tools for correlative cryo-fluorescence microscopy and cryo-electron tomography applied to whole mitochondria in human endothelial cells, *Eur. J. Cell Biol.* **88**, 669-684 (2009).
- [16] D. Nicastro, A. S. Frangakis, D. Typke, and W. Baumeister, Cryo-electron tomography of neurospora mitochondria, *J. Struct. Biol.* **129**, 48-56 (2000).
- [17] M. Van Gorp, N. Festjens, G. Van Loo, X. Saelens, and P. Vandenabeele, Mitochondrial intermembrane proteins in cell death, *Biochem. Biophys. Res. Comm.* **304**, 487-497 (2003).
- [18] L. Griparic, N. N. Van Der Wel, I. J. Orozco, P. J. Peters, and A. M. Van Der Blik, Loss of the intermembrane space protein Mgm1/OPA1 induces swelling and localized constrictions along the lengths of mitochondria, *J. Biol. Chem.* **279**, 18792-18798 (2004).
- [19] J. Friedman and G. K. Voeltz, The ER in 3D: a multifunctional dynamic membrane network, *Trends Cell Biol.* **21**, 709-717 (2011).
- [20] M. Joensuu, I. Belevich, O. Rämö, I. Nevzorov, H. Vihinen, M. Puhka, T. M. Witkos, M. Lowe, M. K. Vartiainen, and E. Jokitalo, ER sheet persistence is coupled to myosin 1c-regulated dynamic actin filament arrays, *Mol. Biol. Cell* **25**, 1111-1126 (2014).
- [21] Y. Shibata, T. Shemesh, W. A. Prinz, A. F. Palazzo, M. M. Kozlov, and T. A. Rapoport, Mechanisms determining the morphology of the peripheral ER, *Cell* **143**, 774-788 (2010).
- [22] J. Soboloff, M. Madesh, and D. L. Gill, Sensing cellular stress through STIM proteins, *Nature Chem. Biol.* **7**, 488 (2011).
- [23] M. J. Dayel, E. F. Y. Hom, and A. S. Verkman, Diffusion of green fluorescent protein in the aqueous-phase lumen of endoplasmic reticulum, *Biophys. J.* **76**, 2843-2851 (1999).
- [24] Y. Okubo, J. Suzuki, K. Kanemaru, N. Nakamura, T. Shibata, and M. Iino, Visualization of Ca²⁺ filling mechanisms upon synaptic inputs in the endoplasmic reticulum of cerebellar purkinje cells, *J. Neurosci.* **35**, 15837-15846 (2015).
- [25] A. S. Verkman, Solute and macromolecule diffusion in cellular aqueous compartments, *Trends Biochem. Sci.* **27**, 27-33 (2002).
- [26] M. Terasaki, T. Shemesh, N. Kasthuri, R. W. Klemm, R. Schalek, K. J. Hayworth, A. R. Hand, M. Yankova, G. Huber, J. W. Lichtman, and others, Stacked endoplasmic reticulum sheets are connected by helicoidal membrane motifs, *Cell* **154**, 285-296 (2013).
- [27] J.-P. Kessler, Control of cleft glutamate concentration and glutamate spill-out by perisynaptic glia: uptake and diffusion barriers, *PLoS One* **8**, e70791 (2013).
- [28] A. V. Tzingounis and J. I. Wadiche, Glutamate transporters: confining runaway excitation by shaping synaptic transmission, *Nat. Rev. Neurosci.* **8**, 935 (2007).
- [29] M. A. Herman and C. E. Jahr, Extracellular glutamate concentration in hippocampal slice, *J. Neurosci.* **27**, 9736-9741 (2007).
- [30] P. J. Mulholland, E. P. Carpenter-Hyland, M. C. Hearing, H. C. Becker, J. J. Woodward, and L. J. Chandler, Glutamate transporters regulate extrasynaptic NMDA receptor modulation of Kv2.1 potassium channels, *J. Neurosci.* **28**, 8801-8809 (2008).
- [31] C. R. Rose, L. Felix, A. Zeug, D. Dietrich, A. Reiner, and C. Henneberger, Astroglial Glutamate Signaling and Uptake in the Hippocampus, *Front. Mol. Neurosci.* **10**, 451 (2017).
- [32] O. J. Castejón, The extracellular space in the edematous

- human cerebral cortex: an electron microscopic study using cortical biopsies, *Ultrastruct. Pathol.* **33**, 102-111 (2009).
- [33] J. P. Kinney, J. Spacek, T. M. Bartol, C. L. Bajaj, K. M. Harris, and T. J. Sejnowski, Extracellular sheets and tunnels modulate glutamate diffusion in hippocampal neuropil, *J. Compar. Neurology* **521**, 448-464 (2013).
- [34] M. Smoluchowski, Versuch einer Mathematischen Theorie der Koagulations Kinetik Kolloider Lousungen, *Z. Phys. Chem.* **129**, 129-168 (1917).
- [35] F. C. Collins and G. E. Kimball, Diffusion-controlled reaction rates, *J. Colloid Sci.* **4**, 425-437 (1949).
- [36] R. Samson and J. M. Deutch, Exact solution for the diffusion controlled rate into a pair of reacting sinks, *J. Chem. Phys.* **67**, 847 (1977).
- [37] R. Samson and J. M. Deutch, Diffusion-controlled reaction rate to a buried active site, *J. Chem. Phys.* **68**, 285-290 (1978).
- [38] H. Sano and M. Tachiya, Partially diffusion-controlled recombination, *J. Chem. Phys.* **71**, 1276 (1979).
- [39] D. C. Torney and H. M. McConnell, Diffusion-Limited Reaction Rate Theory for Two-Dimensional Systems, *Proc. Royal Soc. London A* **387**, 147-170 (1983).
- [40] O. G. Berg and P. H. von Hippel, Diffusion-Controlled Macromolecular Interactions, *Ann. Rev. Biophys. Biophys. Chem.* **14**, 131-160 (1985).
- [41] H.-K. Tsao, S.-Y. Lu, and C.-Y. Tseng, Rate of diffusion-limited reactions in a cluster of spherical sinks, *J. Chem. Phys.* **115**, 3827-3833 (2001).
- [42] S. D. Traytak and W. Price, Exact solution for anisotropic diffusion-controlled reactions with partially reflecting conditions, *J. Chem. Phys.* **127**, 184508 (2007).
- [43] W. Strieder, Diffusion-controlled reaction on an elliptic site, *J. Chem. Phys.* **130**, 176103 (2009).
- [44] C. Eun, P. M. Kekenus-Huskey, and J. A. McCammon, Influence of neighboring reactive particles on diffusion-limited reactions, *J. Chem. Phys.* **139**, 044117 (2013).
- [45] J. A. Biello and R. Samson, Competitive effects between stationary chemical reaction centres: A theory based on off-center monopoles, *J. Chem. Phys.* **142**, 094109 (2015).
- [46] D. S. Grebenkov, R. Metzler, and G. Oshanin, Effects of the target aspect ratio and intrinsic reactivity onto diffusive search in bounded domains, *New J. Phys.* **19**, 103025 (2017).
- [47] D. S. Grebenkov, R. Metzler, and G. Oshanin, Towards a full quantitative description of single-molecule reaction kinetics in biological cells, *Phys. Chem. Chem. Phys.* **20**, 16393-16401 (2018).
- [48] D. Shoup, G. Lipari and A. Szabo, Diffusion-controlled bimolecular reaction rates. The effect of rotational diffusion and orientation constraints, *Biophys. J.* **36**, 697-714 (1981).
- [49] D. S. Grebenkov and G. Oshanin, Diffusive escape through a narrow opening: new insights into a classic problem, *Phys. Chem. Chem. Phys.* **19**, 2723-2739 (2017).
- [50] S. D. Traytak, Diffusion-controlled reaction rate to an active site, *Chem. Phys.* **192**, 1-7 (1995).
- [51] J. S. Gill, C. M. Salafia, D. S. Grebenkov, and D. D. Vvedensky, Modelling oxygen transport in human terminal villi, *J. Theor. Biol.* **291**, 33-41 (2011).
- [52] D. S. Grebenkov, Universal formula for the mean first passage time in planar domains, *Phys. Rev. Lett.* **117**, 260201 (2016).
- [53] B. Sapoval, General Formulation of Laplacian Transfer Across Irregular Surfaces, *Phys. Rev. Lett.* **73**, 3314 (1994).
- [54] D. S. Grebenkov, *Partially Reflected Brownian Motion: A Stochastic Approach to Transport Phenomena*, in "Focus on Probability Theory", Ed. L. R. Velle, pp. 135-169 (Nova Science Publishers, 2006).
- [55] D. S. Grebenkov, Residence times and other functionals of reflected Brownian motion, *Phys. Rev. E* **76**, 041139 (2007).
- [56] A. Singer, Z. Schuss, A. Osipov, and D. Holcman, Partially Reflected Diffusion, *SIAM J. Appl. Math.* **68**, 844 (2008).
- [57] P. C. Bressloff, B. A. Earnshaw, and M. J. Ward, Diffusion of protein receptors on a cylindrical dendritic membrane with partially absorbing traps, *SIAM J. Appl. Math.* **68**, 1223 (2008).
- [58] S. Traytak, The diffusive interaction in diffusion-limited reactions: the steady-state case, *Chem. Phys. Lett.* **197**, 247-254 (1992).
- [59] M. Galanti, D. Fanelli, S. D. Traytak, and F. Piazza, Theory of diffusion-influenced reactions in complex geometries, *Phys. Chem. Chem. Phys.* **18**, 15950 (2016).
- [60] S. D. Traytak and D. S. Grebenkov, Diffusion-influenced reaction rates for active "sphere-prolate spheroid" pairs and Janus dimers, *J. Chem. Phys.* **148**, 024107 (2018).
- [61] M. Felici, M. Filoche, and B. Sapoval, Diffusional screening in the human pulmonary acinus, *J. Appl. Physiol.* **94**, 2010 (2003).
- [62] I. N. Sneddon, *Mixed Boundary Value Problems in Potential Theory* (Wiley, NY, 1966).
- [63] T. H. Hill, Effect of rotation on the diffusion-controlled rate of ligand-protein association, *Proc. Natl. Acad. Sci. USA* **72**, 4918-4922 (1975).
- [64] A. M. Berezhkovskii and A. V. Barzykin, Simple formulas for the trapping rate by nonspherical absorber and capacitance of nonspherical conductor, *J. Chem. Phys.* **126**, 106102 (2007).